Steel and Composite Structures, *Vol. 29, No. 6 (2018) 731-744*
DOI: https://doi.org/10.12989/scs.2018.29.6.731

Cyclic behaviour of concrete encased steel (CES) column-steel beam joints with concrete slabs

Liusheng Chu [1], Danda Li [*2], Xing Ma [2] and Jun Zhao [1]

[1] *School of Civil Engineering, Zhengzhou University, Zheng Zhou, Henan Province, China*
[2] *School of Natural and Built Environments, University of South Australia, Adelaide, SA, Australia*

(*Received August 20, 2018, Revised December 2, 2018, Accepted December 27, 2018*)

Abstract. In this paper, the cyclic behavior of steel beam-concrete encased steel (CES) column joints was investigated experimentally and numerically. Three frame middle joint samples with varying concrete slab widths were constructed. Anti-symmetrical low-frequency cyclic load was applied at two beam ends to simulate the earthquake action. The failure modes, hysteretic behavior, ultimate load, stiffness degradation, load carrying capacity degradation, displacement ductility and strain response were investigated in details. The three composite joints exhibited excellent seismic performance in experimental tests, showing high load-carrying capacity, good ductility and superior energy dissipation ability. All three joint samples reached their ultimate loads due to shear failure. Numerical results from ABAQUS modelling agreed well with the test results. Finally, the effect of the concrete slab on ultimate load was analyzed through a parametric study on concrete strength, slab thickness, as well as slab width. Numerical simulation showed that slab width and thickness played an important role in the load-carrying capacity of such joints. As a comparison, the influence of concrete grade was not significant.

Keywords: beam-column joint; concrete encased steel (CES) column; steel beam with concrete slabs; cyclic loads; shear capacity; moment capacity

1. Introduction

The concept of concrete encased steel (CES) structures firstly appeared as a concrete encased beam in Iowa bridges in 1894. It is a typical composite component with structural steel embedded in reinforced concrete. The CES applications in Japan were also recorded as steel-reinforced concrete (SRC). Apart from traditional CES-column-CES beam frame structures, hybrid structural types such as CES column–steel beam systems, CES column-composite floor systems provided alternative economic choices in current industrial practise (Begum *et al*. 2013). A famous example is the 492m high Shanghai World Financial Center, the main structure of which is a hybrid system with a reinforced concrete core combined with a series of CES column–steel beam frames. In general, CES has the combined advantageous properties from structural steel and reinforced concrete and is widely used in high rise buildings, large-span bridges and transmission towers. CES has improved properties of better fire-resistance over traditional steel structures and higher stiffness, stronger seismic capacity, better ductility, lighter weight, easier construction over traditional concrete structures. Recent structural applications in civil and infrastructure engineering have proved that CES has good potential in the future market, especially in the seismic areas (Lagaros and Magoula 2013).

The current research on CES structures mainly focuses on the performance of structure elements (Shanmugam and Lakshmi 2011). Pisano *et al*. (2013) studied the peak loads and failure modes of steel-reinforced concrete beams and presented the prediction formulas by limit analysis method. Orr *et al*. (2014) investigated the shear capacity of a steel-reinforced concrete beam and indicated that some design code might result in an unconservative shear design for non-prismatic sections. Chen *et al*. (2016) and Chen and Liu (2018) experimentally studied the axial compression ratio limit and hysteretic performance of cross shaped CES columns and demonstrated good ductility and deformation capacity of such structural components.

In composite structures with CES columns, beam-column joints are crucial for overall structural strength and stiffness capacity. They are key components for load transferring and moment distribution, thus significantly affect structural seismic performance. Xu *et al*. (2015) studied the seismic-induced damage of 3D joints connected with T-shaped CES column-steel beams. The damage index calculation models were developed. Effects of steel configuration, loading angle and axial compression ratio on damage development were investigated after considering three dimensional interaction through Park-Ang model. Wang *et al*. (2015, 2016) developed a type of enlarged cross-shaped CES columns with an improved concrete confinement effect. The experimental investigation verified that the new CES joints had improved shear capacity. Zhang and Jia (2016) investigated the seismic behavior of both CES columns with ultra-high strength concrete and normal CES columns in frame structure under low reversed cycle

∗Corresponding author, Ph.D., Research Fellow,
E-mail: danda.li@unisa.edu.au

http://www.techno-press.org/?journal=scs&subpage=6
ISSN: 1229-9367 (Print), 1598-6233 (Online)

lateral loading. The results showed that using encased steel and high-strength stirrups in the ultra-high strength concrete could alleviate the brittleness problem and enhance both strength capacity and ductility. Better seismic behaviour of SRUHSC was reported than normal CES. Xiang *et al*. (2017) experimentally investigated seismic behavior of T-shaped CES column-reinforced concrete beam joints which showed good performance under seismic loads with satisfactory shear-resistant capacity and ductility. Yan *et al*. (2017) developed an analytical hysteretic model for CES column-CES beam joint under cyclic loads. The effect of the loading cycle number was studied. In 2018, Ma *et al*. studied cyclic behaviour of CES column-steel beam joints with normal concrete and recycled coarse aggregated concrete and indicated that the recycled coarse aggregates reduced joint shear capacity by up to 10%. Most of the above research focused on structures composed of CES columns-reinforced concrete beams or CES columns-CES beams. For a widely used structural type with CES-columns and steel beams, there is still a research gap on its joint analysis.

2. Research significance

The authors attempt to investigate the structural response of CES column-steel beam joints with concrete slabs subject to cyclic loads through experimental studies and numerical simulations. The failure mechanism, load-displacement relationship, load carrying capacity as well as stiffness degradation are studied. The effect of the concrete slab is analysed through a parametric study on concrete grade, slab thickness and width. The authors expect that this research can provide perspective on the effectiveness of this structural joint concept and stimulate its applications in industrial practise.

3. Experimental program

3.1 Specimen

In a frame structure, middle columns usually carry more seismic loads such as normal force and bending moment than an edge column. As a result, middle frame joints tend to be more critical due to their complicated loading and connecting situations than an edge joint. In this paper, the tested CES column-steel beam and CES-column-composite beam joints were designed as the middle joint of a frame structure (within the region of beam and column contra-flexure point) according to Chinese standards of JGJ 138-2001 and YB 9082-2006. A half scale model was used for this investigation. A total of three samples were casted for testing. One of them is CES column-steel beam joint (CES1) and two are CES column-composite beam joints (CES2 and CES3).

Steel section is Q235 graded with tested yield strength 303 MPa and ultimate strength 407 MPa. Longitudinal reinforcing bars of both column and slab are HRB335 graded with tested yield strength 379 MPa and ultimate strength 534 MPa. The stirrups in the column and secondary direction bars in the slab are HPB300 graded with tested yield strength 316 MPa and ultimate strength 432 MPa. Concrete compressive strength is C30 with the material properties shown in Table 1.

The geometry of the structure is shown below: column

Table 1 Concrete material properties

Sample ID	f_{cu}^{k} (MPa)	f_{ck} (MPa)	f_{tk} (MPa)	E_c (MPa)
H-1	31.1	21.8	2.1	30166
H-2	32.6	21.8	2.1	30646
H-3	33.9	22.7	2.2	31024
Average	32.6	22.1	2.1	30612

Table 2 Cross section and reinforcement details

Sample ID	Longitudinal bars in column	Stirrup bars in column	Slab width (mm)	Longitudinal bars in slab	Secondary bars in slab
CES-1	4Φ12	Φ8@100	N/A	N/A	N/A
CES-2	4Φ12	Φ8@100	800	8Φ12	Φ8@120
CES-3	4Φ12	Φ8@100	1000	10Φ12	Φ8@120

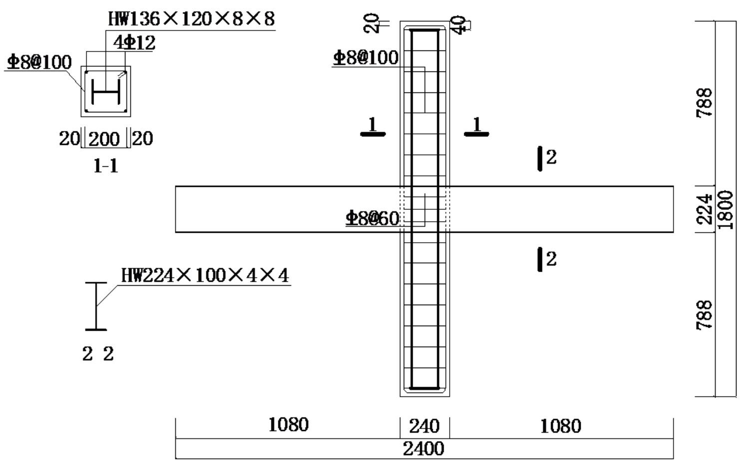

Fig. 1 Column-steel beam joint CES1(unit: mm)

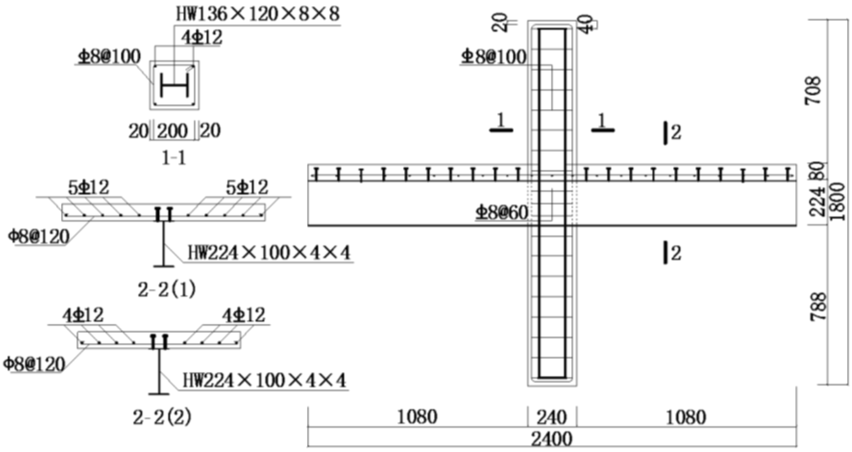

Fig. 2 Column-composite beam joints of CES2 and CES3 (unit: mm)

(a) CES column-steel beam joint (CES1)

(b) CES column-composite beam joint with shear studs(CES2 and CES3)

(c) Slab reinforcement arrangement

Fig. 3 Hybrid joints under construction

is 1.8 m tall, beam span is 2.4 m, the concrete slab is 80 mm thick. For all three joints, the concrete column cross section size is 240 mm × 240 mm, reinforced steel in the column is at the size of 136 × 120 × 8 × 8 in mm and steel beam is sized at 224 × 100 × 4 × 4 in mm. Table 2 lists the reinforcement and slab details of the three joint specimens. Figs. 1 and 2 show the details of the three specimens.

The steel beams were welded to the reinforced steel core of the column on both sides. Stiffeners were used to strengthen the intersecting area. 8 mm stiffeners were applied at beam loading ends to avoid large local deformation. 60 A13 shear studs were welded to beam top

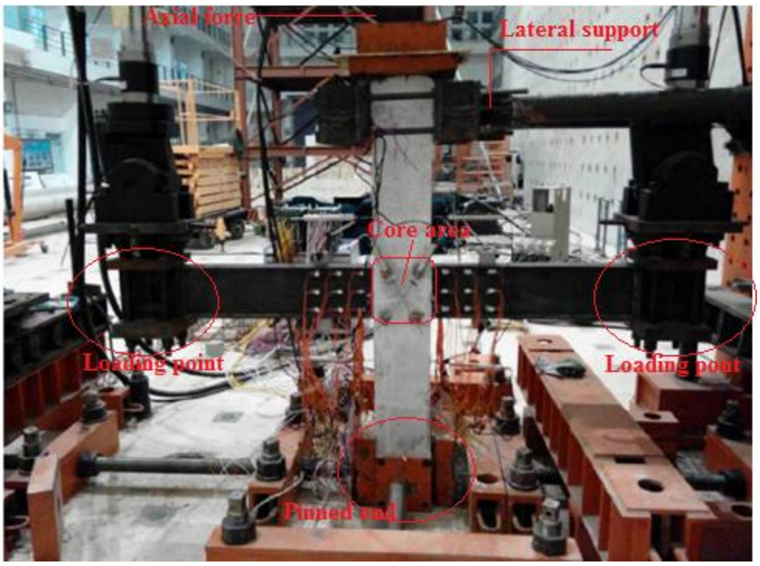

(a) Sample in lab

Fig. 4 Test set-up for sample CES1

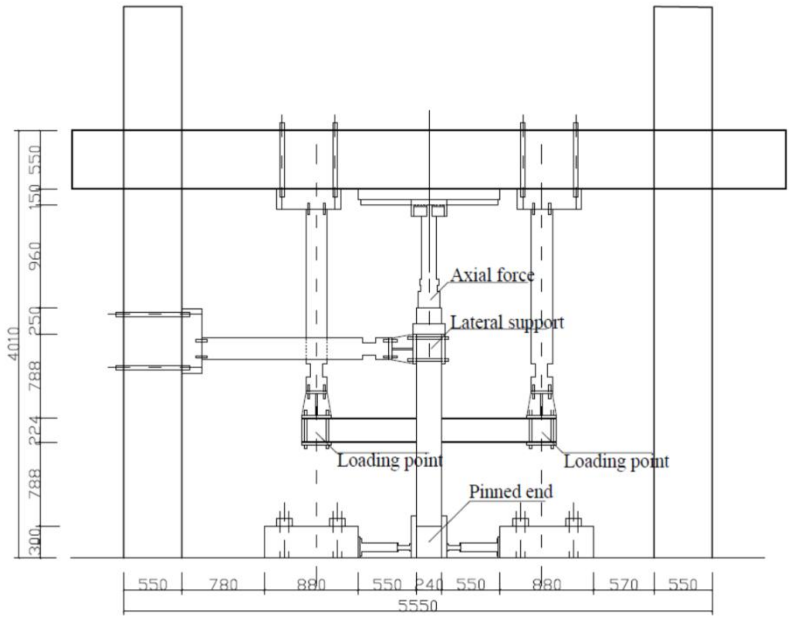

(b) Test set up sketch

Fig. 4 Continued

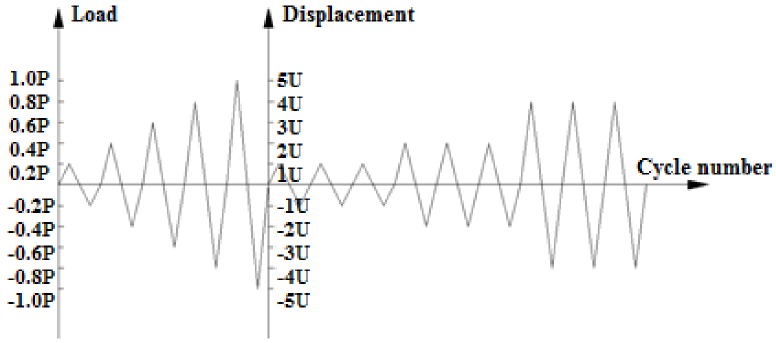

Fig. 5 Loading scheme for cyclic tests

to provide a rigid connection between the steel beam and concrete slab. Fig. 3 shows the column, beam, reinforcement set up during sample casting. Concrete was casted in different layers and the electrical vibrator was used to ensure concrete is well compacted and placed. Shear studs in sample CES2 and CES3 were spaced at 110 mm along beam length and 60 mm in the cross direction. Edge distance is 42 mm at both ends of the beam.

3.2 Loading schemes and measurements

The test setup for specimen CES1 is shown in Fig. 4, where the column was fixed at the bottom end on a ground beam through high-strength bolts and the top column end was laterally restrained. Vertical loads were applied at both beam ends through actuators. Column compressive capacity N_u, the yield capacity of the vertical beam loads P_y and the corresponding yielding displacement u were calculated through FEM simulation before tests. A constant axial load of 40%N_u was applied at column top through a hydraulic loading system. Beam end loads were under a combined displacement-control and force-control loading procedure as shown in Fig. 5. In general, the force control method is more accurate than the displacement controlling procedure before yielding due to the relatively small displacement within this stage. However after yielding, applied loads might drop with increasing displacement, thus displacement control would be more ideal. The loading procedure followed Chinese standard (JGJ 101-96), where the force-controlled load was applied at an increment of $0.2P_y$, until it reached P_y with one cycle per loading step. Beyond yielding, a displacement-control load with an increment of u was employed with three cycles per loading step. Test stopped when the applied loads dropped to 85% of peak capacity value. The downward load is defined as the positive force. During loading procedure, the loads at the two beam ends were kept in opposite directions, i.e., the positive load at the right end is accompanied by a negative load at the left end or in the opposite way. The main measurements include the applied load, beam end displacement, strain distribution, crack development at joint core area (Figs. 4 and 6).

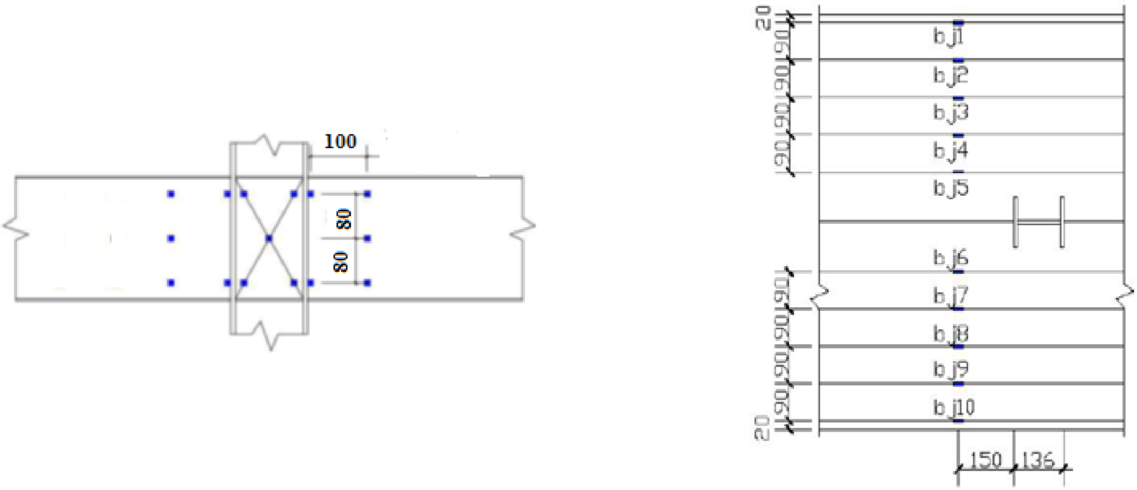

(a) Strain gauge on steel beam (b) Strain gauge on slab rebars

Fig. 6 Stain gauge arrangement

4. Test results and analysis

4.1 The failure mode of CES1

Fig. 7 shows the crack development in CES1 during loading. The first minor crack appeared at the load of 21 kN with a length of 40 mm. At 42 kN the bottom flange of beam reached yielding strain indicating that the beam entered the plastic stage. Displacement controlled loading was then applied, when load reached 2 times yielding displacement, more cracks occurred and crack width developed faster. After displacement past 3 times the yielding displacement, no more new cracks appeared, the existing cracks kept propagating. In the core area, concrete started spalling off. At 4 times yielding displacement, one of the strain displacement sensors dropped off, concrete at the ends of two main diagonal cracks started spalling off, concrete at the column/beam flanges connection area started crushing, shear deformation was very obvious, buckling at beam bottom flange was observed. At 5 times yielding displacement, obvious and substantial buckling at beam flanges was observed with concrete crushing at core area, load dropped below 85% of peak value, loading was then stopped. The final failure mode of CES1 was shown in Fig. 8.

4.2 Failure modes of CES2 and CES3

The first crack in CES2 occurred due to tensile failure at column side face at a load of 39 kN (Fig. 9) and then started to develop in the diagonal direction. With load increasing, some minor cracks occurred at slab surfaces near the column. At a load of 52 kN, many new diagonal cracks appeared in the core area. Hysterestic curve showed a turning point at the load of 65 kN with existing cracks keeping extending and the bottom flange of the steel beam reached yielding. Then the displacement controlled load was applied. At 2 times yielding displacement concrete started spalling and more cracks occurred in the core area at the width of about 0.5 mm. A longitudinal crack appeared extending from column face to beam end. At 3 times yielding displacement, more minor cracks occurred at four corners in the core area with the maximum width of 1.5 mm. At 4 times yielding displacement, concrete at column/beam bottom flanges started crushing. At 5 times

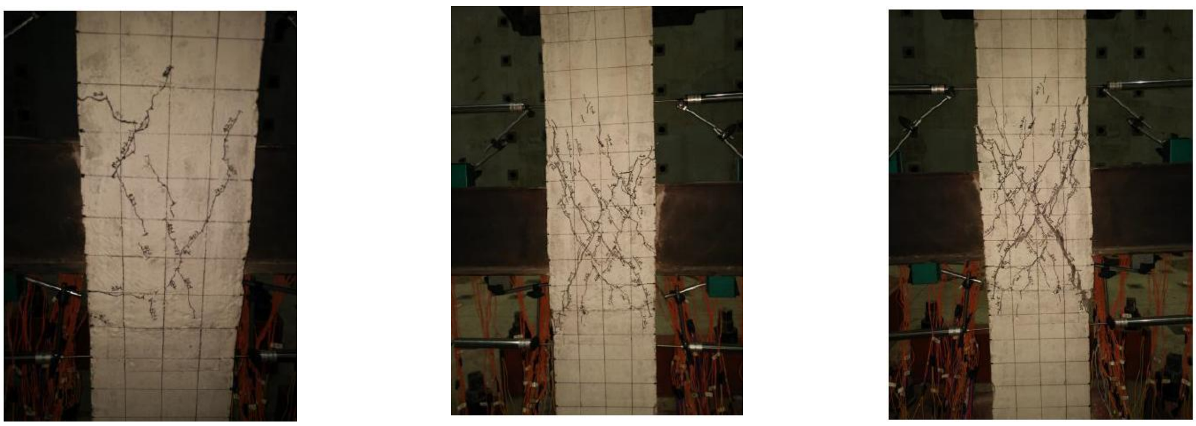

(a) Yield displacement (b) 3 times yield displacement (c) 4 times yield displacement

Fig. 7 Crack development on column side at different loading steps (displacement control)

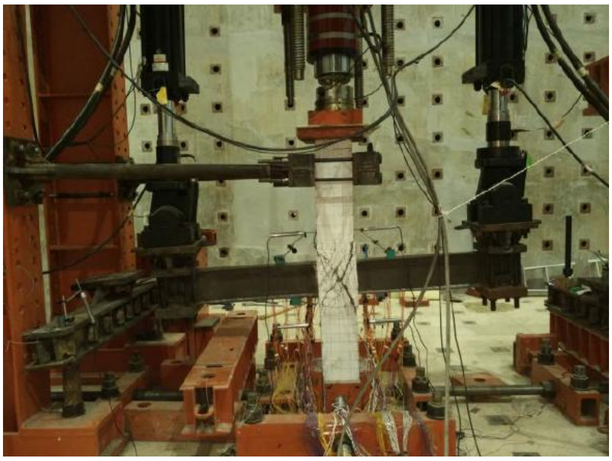

Fig. 8 The failure mode of CES1

yielding displacement, beam bottom flange started buckling, concrete in the core area started spalling, shear deformation became obvious, more cracks appeared at slab top and bottom surface and load bearing capacity dropped. At 6 times yielding deformation, load bearing capacity continued dropping, obvious slip between steel bottom flange and column face occurred. Severe concrete spalling and buckling at steel beam bottom flange occurred. Fig. 9 shows the failure modes and final crack distributions of CES2. CES3 experienced similar cracking development to CES2 and its failure mode is shown in Fig. 10.

There was no obvious welding failure between the steel beam and column steel core, neither fracture nor buckling occurred for the steel beam/shear stud connection. In this investigation, CES1 underwent shear deformation failure, without very obvious beam bottom flange buckling (Fig. 8). CES2 and CES3 failed under the cyclic loading with severe shear deformation and obvious beam bottom flange buckling. The reason is due to the composite effect of concrete slabs in CES2 and CES3 (Fig. 10(c)), which caused the section neutral axis moving up and increased the compressive stress in the bottom flange of the beam with more obvious buckling occurred under low-frequency cyclic load.

4.3 Hysteretic curves

The load-displacement relationships at the right beam end for CES1, CES2 and CES3 are shown in Figs. 11-13. Wide hysteretic curves were obtained for all three specimens. It indicates great energy dissipation ability and potentially good performance for the seismic load. From the

(a) System final failure mode

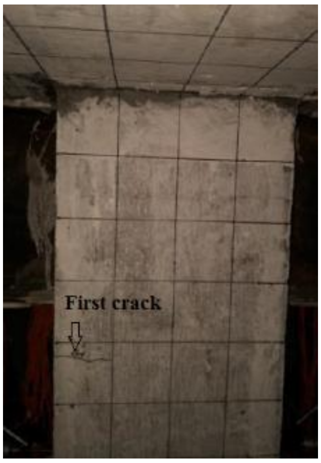

(b) First crack on column

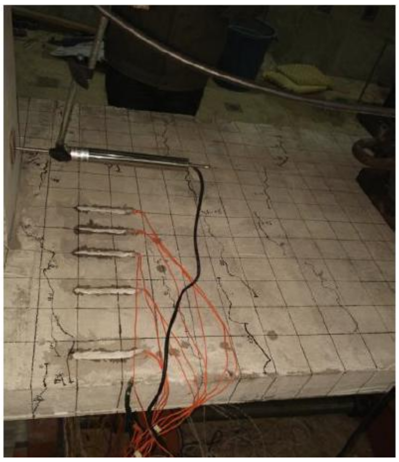

(c) Crack on top slab surface

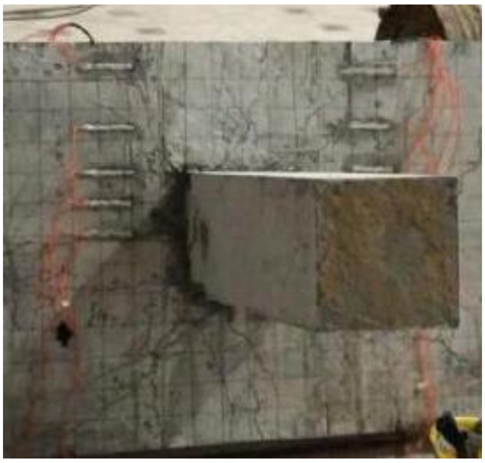

(d) Crack on the bottom slab surface

Fig. 9 The failure mode and cracking development of CES2

(a) Cracks on top slab surface (b) Cracks on bottom slab surface (c) Bottom flange buckling of steel beam

Fig. 10 The failure mode of CES3

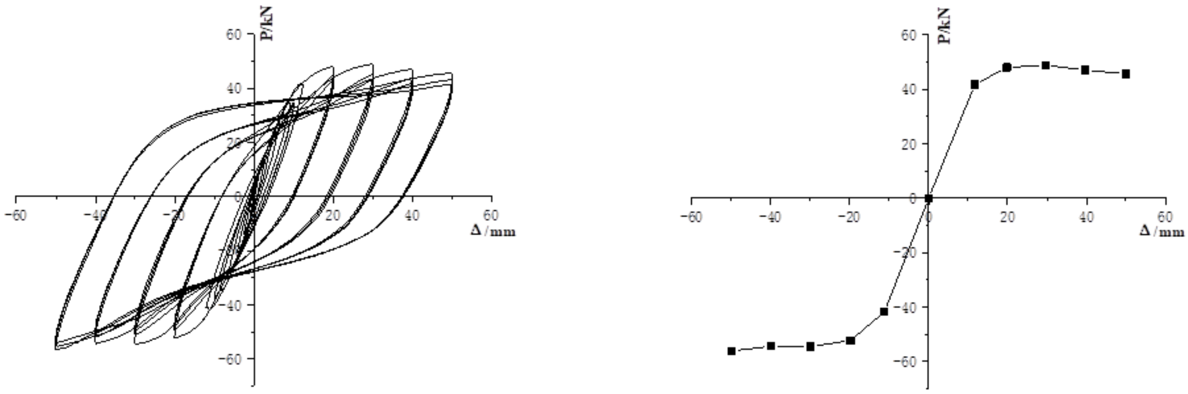

Fig. 11 Hysteretic curves and hysteresis envelope curve of CES1

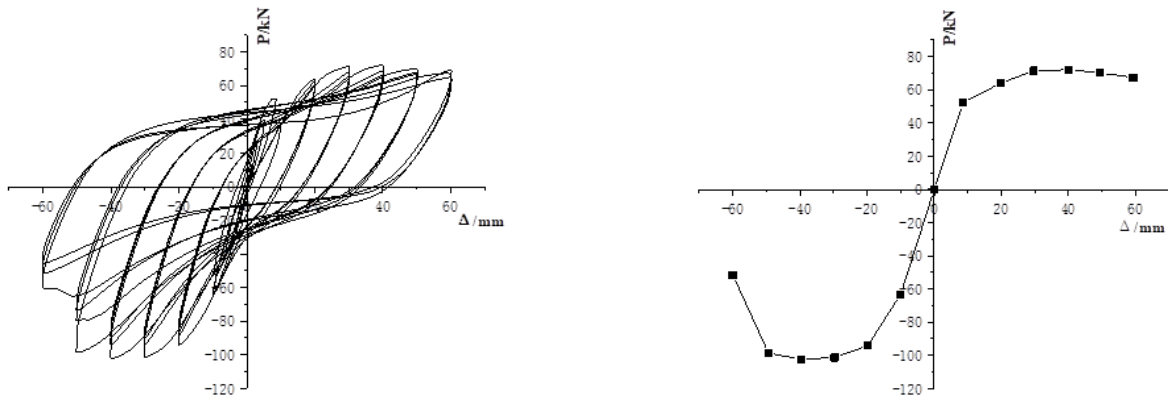

Fig. 12 Hysteretic curves and hysteresis envelope curve of CES2

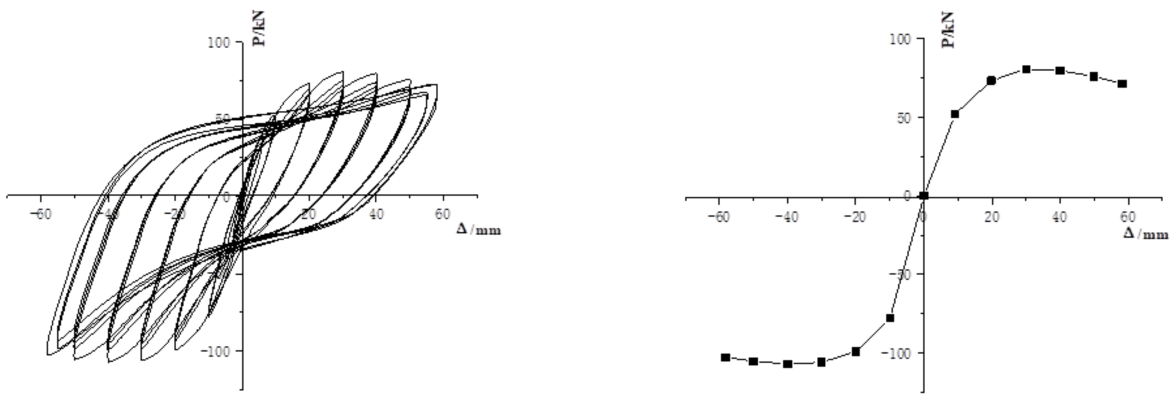

Fg. 13 Hysteretic curves and hysteresis envelope curve of CES3

loading and unloading curve slopes, it demonstrates that there is a little stiffness loss after many cycles of load where the stiffness degradation in the negative direction is more obvious than in the positive direction. The reason is due to the compressive contribution from a concrete slab when downward applied load causes negative bending moments. Due to the higher cyclic effect on concrete, more stiffness degrading occurred during the negative loading procedure. The compressive contribution from concrete slab also explains the phenomenon that the hysteresis curves are not symmetrical about the horizontal axis. The curves for CES2 and CES3 are not as wide as for CES1, however, higher load bearing capacity was observed for these two specimens. It was also found that the bearing capacity increases with higher slab width. Figs. 11-13 also present the envelope curve of CES1, CES2 and CES3. The envelope curves of the three specimens are all s-shaped, which indicates three stages: elastic stage, plastic stage and ultimate failure stage. The gently decreasing post-peak part showed good plastic deformation ability and good ductility of the specimens.

The main characteristics in envelope curve include yield load, yield displacement, peak load, peak displacement, failure load and ultimate displacement. Table 3 lists the characteristic load for the three specimens. Due to the contribution from the reinforced concrete slab, CES2 and CES3 showed higher positive and negative load carrying capacity. Compared with ECS1, the yielding capacity of both CES2 and CES3 increased from 41.7 kN to 52.1 kN for an upward load with increasing percentages of 25%. For a downward load, the yielding capacity increased from 41.8 kN to 63.3 kN (CES2) and 77.7 KN (CES3) with increasing rates of 51% and 86%, respectively. The increasing rates for peak upward load are 48% for ECS2 and 65% for CES3. For the peak downward load, the increasing rates are 87% and 96%, respectively. Compared to CES2, both positive and negative load carrying capacity are higher for CES3 due to the larger slab width.

Table 4 presents the displacement characteristics for the three specimens. Compared with CES1, the ultimate displacements due to upward loads for CES2 and CES3 increased from 45.7 mm to 59.3 mm and 58.2 mm, with increasing rates of 30% and 27%, respectively. Similar increments occur for the case of downward loads, the increasing rates are 20% and 17%. Defining the ductility factor as the ratio between the ultimate displacement and the yielding displacement, the average ductility factor is between 3.9 and 6.9. CES2 and CES3 showed very close ductility factor which is about 40% higher than CES1.

4.4 Load carrying capacity and stiffness degrading

The overall bearing capacity degrading factor K_i at the i^{th} loading step is defined as

$$K_i = \frac{P_i}{P_{\max}} \tag{1}$$

Where P_i is the peak load applied at the ith loading step; $P_{\max}$ is the maximum applied load during the whole test. The relationship between K_i and maximum displacement d at the i^{th} step is shown in Fig. 14 showing a gentle decreasing trend without obvious degrading of capacity, where d_y is the displacement at initial yielding.

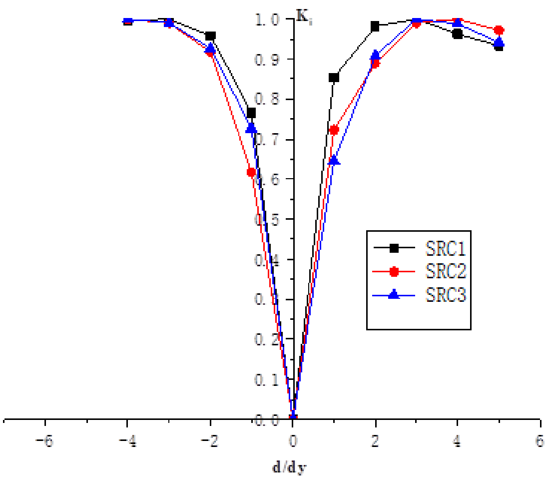

Fig. 14 Load carrying capacity degrading factor

Table 3 Value of main characteristics in the hysteresis envelope curve

Sample ID	Yield load P_y (kN)		Peak load $P_{\max}$ (kN)		Ultimate load P_u (kN)	
	Up	Down	Up	Down	Up	Down
CES1	41.7	41.8	48.9	54.6	45.7	54.4
CES2	52.1	63.3	72.1	102.3	67.4	87.0
CES3	52.1	77.7	80.8	106.9	71.5	102.7

Table 4 Joint displacement and ductility coefficient

Sample ID	Yield displacement Δ_y (mm)		Peak displacement $\Delta_{\max}$ (mm)		Ultimate displacement Δ_u (mm)		Ductility coefficent μ
	up	down	up	down	up	down	average
CES1	11.67	11.21	29.71	29.92	45.65	49.87	4.18
CES2	8.59	9.99	40.09	39.73	59.31	59.98	5.95
CES3	9.22	9.97	30.01	39.95	58.24	58.21	6.08

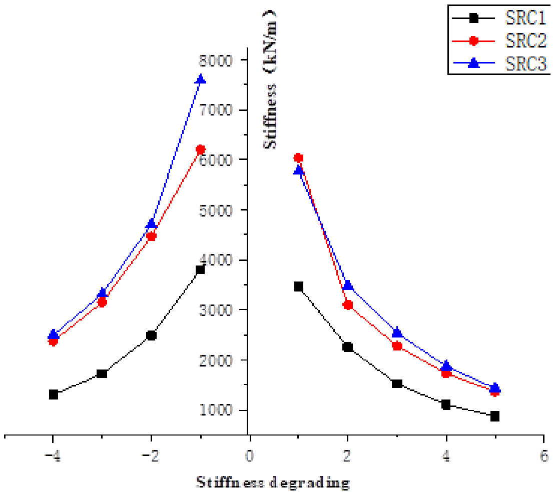

Fig. 15 Stiffness degrading

The stiffness is defined as the ratio of averaged peak load over averaged displacement at peak load points, at the same loading level. As shown in Fig. 15, the stiffness of CES2 and CES3 are larger than that of CES1.CES3 showed slightly larger stiffness than CES2. The similar linear degrading trend was found for all three specimens. For CES2 and CES3, after yielding displacement, the stiffness under negative load was higher than positive load due to the contribution from the concrete slab.

4.5 Energy dissipation capacity

According to Chinese standard JGJ101 (1996), the energy dissipation capacity of the specimen can be expressed through area enclosed by the hysteresis curve. The equivalent viscous damping ratio h_e is defined through an energy dissipation factor E, which is the ratio of the energy dissipated in a hysteresis curve over the energy that an equivalent elastic system needs for the same displacement.

$$h_e = \frac{E}{2\pi} \tag{2}$$

Where $= \frac{S_1}{S_e}$, S_1 and S_e are the shaded areas in the hysteresis curve and the equivalent elastic system as shown in Fig. 16, respectively.

Table 5 lists the energy dissipation capacity S_1, energy dissipation factor E and equivalent viscous damping factor h_e for all three specimens. It is clear that CES2 and CES3 have improved energy dissipation capacity compared with CES1. The energy dissipation capacities at P_{max} point increased from 2267, to 4861 and 4466 kN-mm with increasing percentages of 114% and 97%, respectively. The energy dissipation capacities at the P_u point increase by 52% and 61% for CES2 and CES3, respectively although the viscous damping ratios drop from 0.309 to 0.244 and 0.235. For all three samples, the equivalent viscous damping ratio varied between 0.212-0.309, which was much higher than the composite frame joints with concrete filled steel tubes ranging between 0.11-0.16 (Wang *et al.* 2018).

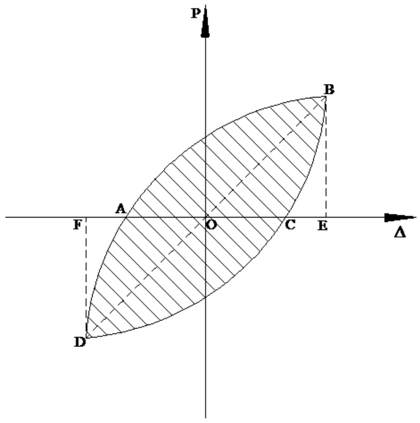

(a) Hysteresis curve

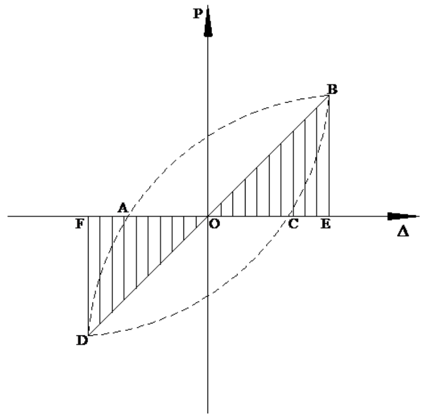

(b) Equivalent elastic system

Fig. 16 Energy dissipation capacity

Table 5 Energy dissipation capacity index

Sample ID	Load	S_1 (kN-mm)	E	h_e
CES1	P_{max}	2267	1.469	0.234
	P_u	4650	1.938	0.309
CES2	P_{max}	4861	1.398	0.223
	P_u	7073	1.535	0.244
CES3	P_{max}	4466	1.334	0.212
	P_u	7480	1.475	0.235

4.6 Strain analysis

Fig. 17 presents the strain distribution along the web height of the steel beam subjected to positively applied loads. It is obvious that the neutral axis of CES 1 is close to the central height at loads below 35 kN. When the load increased, local buckling occurred with large compressive strain at the bottom flange, strain distribution ceased following plane assumption and the neutral axis moved down a little. The neutral axis of CES 3 was above web central height due to the contribution of slab components. Similar to CES 1, the neutral axis in CES 3 moved downward after bottom beam flange buckled. Strains in CES 2 followed the same trend as in CES 3. Fig. 18 shows the strain in different reinforcement at the same slab

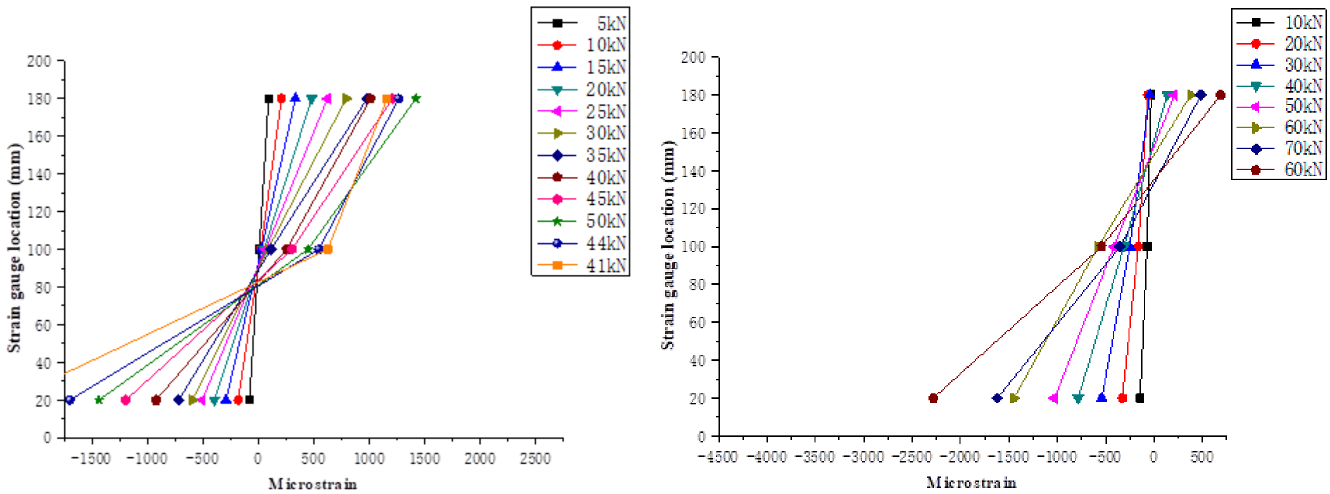

(a) CESI (b) CES 3

Fig. 17 Strain distribution along the height of steel web

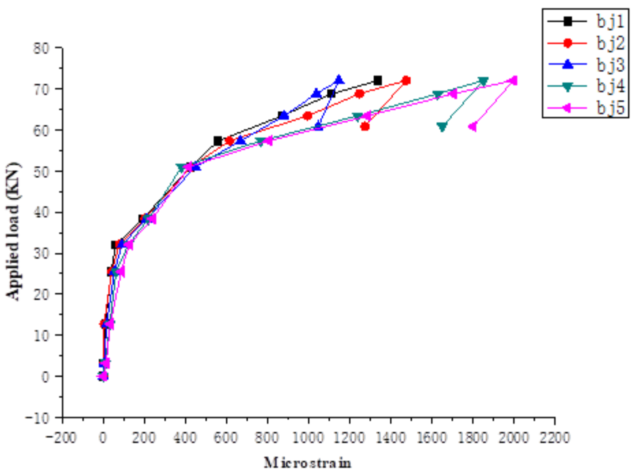

Fig. 18 Strain distribution in slab reinforcement

section. It indicates that the steel strain is uniform along the slab width.

5. FEM modelling

5.1 Model set-up

To better understand the behaviour of the CES column-composite beam structure and also verify the accuracy of the experimental tests, in this research ABAQUS was employed to simulate the structural performance of the CES joints. Concrete damage plasticity model was employed with uniaxial compressive and tensile stress-strain relationship following GB50010-2010, where two failure mechanisms, tensile cracking and compressive crushing were assumed. The compressive and tensile strength were chosen as experimental based values f_{ck} and f_{tk} from Table 2. A simplified bi-linear formula was employed for the stress-strain relationship of steel with tested yielding strength of 303 MPa for Q235, 316 MPa for HPB300 and 379 MPa for HRB335.

Concrete was simulated through reduced linear integrating unit C3D8R. 3D truss element T3D2 was used to model steel reinforcement in both column and slabs. The reinforcement was modelled separately and then 'embedded' in concrete. To simulate local buckling in steel sections, shell element S4 was used to simulate the plate components in steel beam and steel in CES column. The meshed models are shown in Fig. 19.

5.2 FEM results

Fig. 20 gives the hysteretic curve and hysteresis envelope curve for CES 1, which agree well with experimental results. The joint failure modes from FEM also matched well with the experimental study as shown in

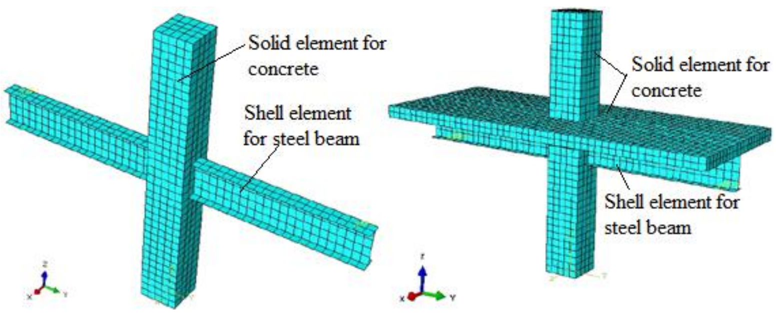

Fig. 19 ABAUQS modelling of CES1 and CES 3

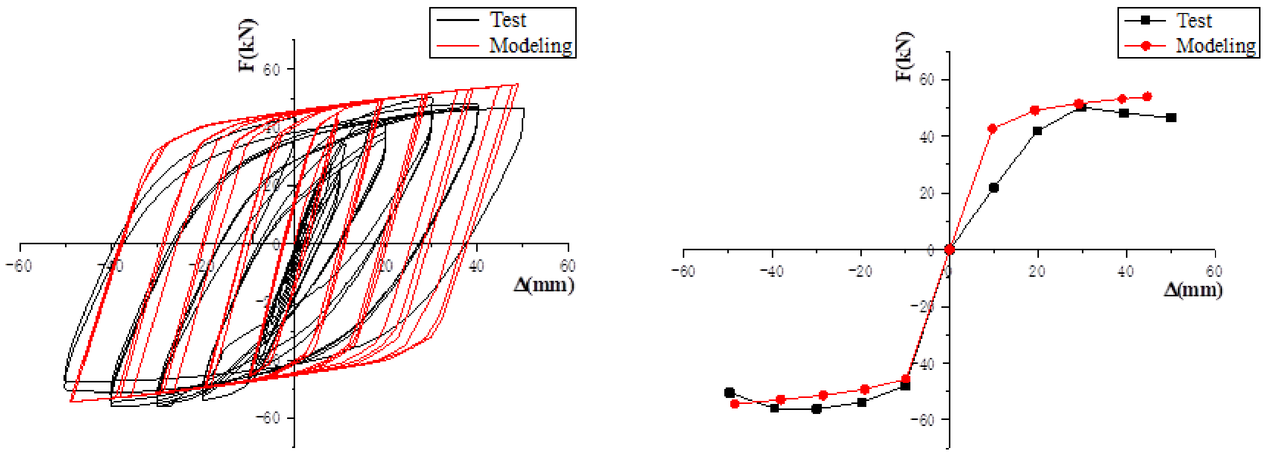

Fig. 20 Hysteretic curves and hysteresis envelope curve of CES1

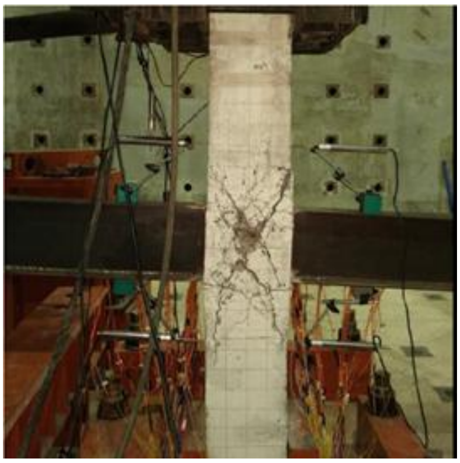

(a) Test

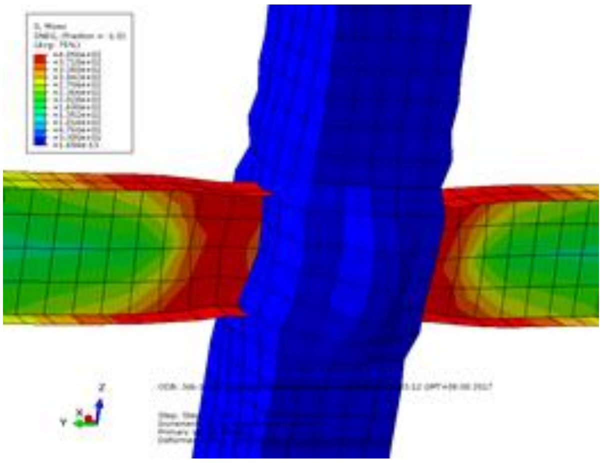

(b) ABAQUS modelling

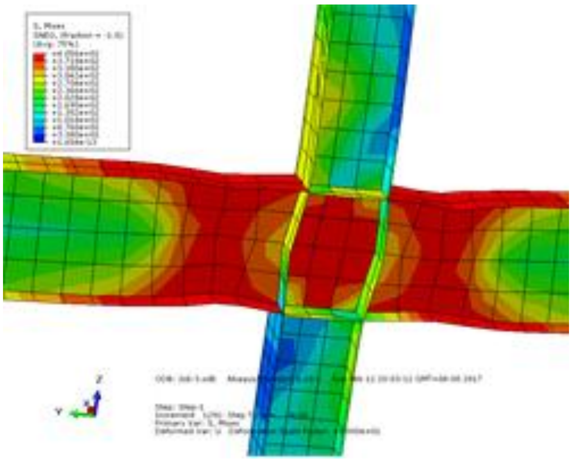

(c) Stress distribution on steel sections at failure point

Fig. 21 Failure mode of specimen CES1

Figs. 21 and 22. Numerical results of concrete stress distribution on slab surfaces were plotted in Fig. 23. The yielding stress zone agree well with failure zone in Fig. 9. The peak loads from FEM were compared with test results for CES1, CES2 and CES3 in Table 6 showing a small difference varying between 1.2 and 4.1%. The comparison above proved that FEM simulation could well predict the structural performance of the frame joints with CES columns and steel beams.

5.3 Influencing of the concrete slab

To study the composite effect from the contribution of the concrete slab, a parametric study was carried out

Table 6 Comparison between numerical modelling and experimental results

Specimen	P_{max} (kN) (up)			P_{max} (kN) (down)		
	Test	Modelling	Error	Test	Modelling	Error
CES 1	48.9	49.5	1.2%	54.6	53.8	1.5%
CES 2	72.1	73.3	1.7%	102.3	98.1	4.1%
CES 3	80.8	82.9	2.6%	106.9	105.2	1.6%

through changing the concrete grade, slab width and thickness based on the main parameters of CES 3. In each of the following cases, only one parameter is different from CES 3. The load capacity P_{max} in terms of the varying parameters is presented in Fig. 24.

It is clear from the above figure that concrete grade has little influence on the load carrying capacity of the joint system. Increasing slab thickness or width could effectively increase both upward and downward load carrying capacity. Due to the significant compressive contribution from slab concrete, slab sizes provide a larger effect on the upward load capacity than downward capacity, where slab concrete is in tension and has little contribution after cracking. The increase in downward loading capacity can be attributed to the contribution from steel rebars embedded in the slab.

6. Conclusions

In this paper, experimental tests were carried out to investigate the cyclic behaviour of a frame joint with CES

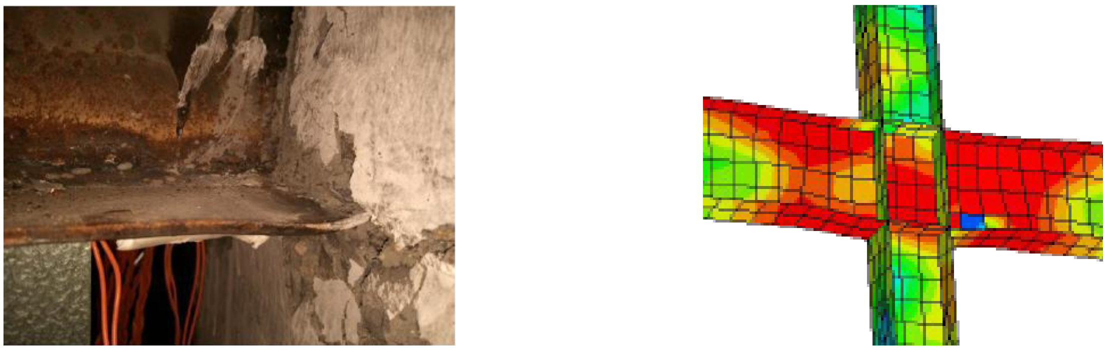

(a) Test (b) ABAQUS modelling

Fig. 22 Buckling mode of the compressive flange in steel beam of CES3

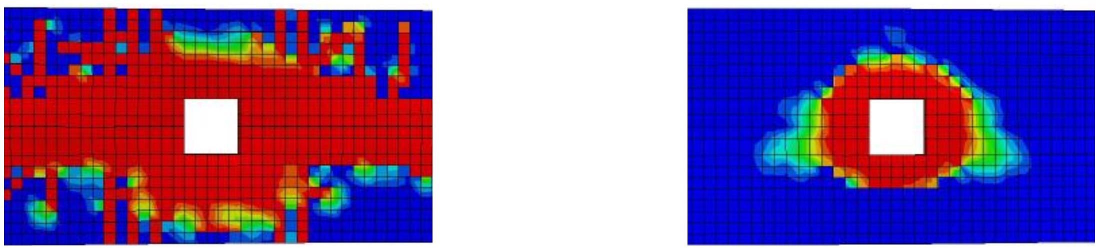

(a) Tensile stress (b) Compressive stress

Fig. 23 Slab concrete stress distribution at failure loading point for CES2

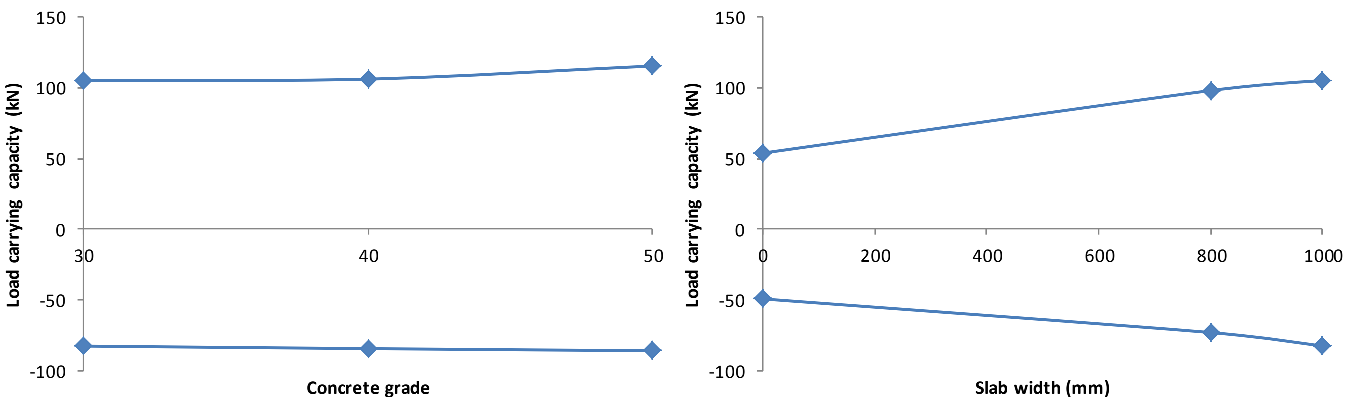

(a) Concrete grade (b) Slab width

Fig. 24 Load-carrying capacity in terms of slab parameters number

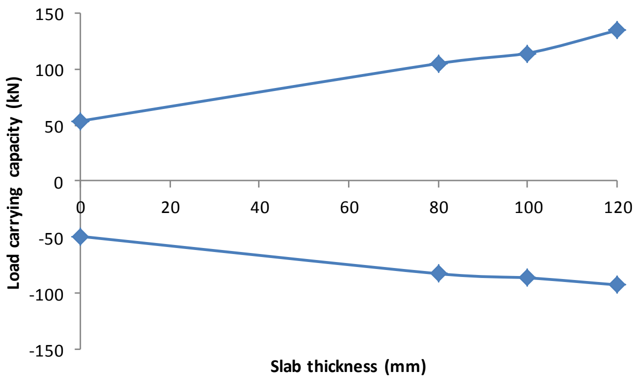

(c) Slab thickness

Fig. 24 Continued

columns and steel or composite beams. The concrete slab effect slab was studied. A series of FEM simulation was conducted. From the experimental study and numerical simulation results, it can be concluded that

(1) The frame joint with CES column and steel or composite beams has good loading carrying capacity, ductility and energy dissipation capacity. It has higher viscous damping ratios when compared with concrete filled steel tube systems;
(2) The combination effect between the concrete slab and steel beam improves structural performance of the composite joints significantly. Compared CES3 and CES1, the load carrying capacity increase by 65% for upward load and 96% for the downward load. The ductility factor increase by 40% and energy dissipation capacity increase by 61%.
(3) Increasing slab width and thickness can effectively improve load carrying capacity with downward loads due to the compressive contribution from concrete slabs. But the improvement drops slightly if with loads in opposite direction. The concrete grade is not a sensitive parameter in the design of this type of joint systems.

Acknowledgments

The authors appreciate the financial support from National Key R&D Program of China (2016YFE0125600); National Natural Science Foundation of China (No. 51408556) and Program for Changjiang Scholarships and Innovative Research Team in University (No. IRT_16R67).

References

Begum, M., Serajus, S.M., Tauhid, B.K.N. and Ahmed, W. (2013), "Cost analysis of steel concrete composite structures in Bangladesh", *Asian J. Civil Eng.*, **14**, 935-944

Chen, Z. and Liu, X. (2018), "Seismic behavior of Steel reinforced concrete cross-shaped column under combined torsion", *Steel Compos. Struct., Int. J.*, **26**(4), 407-420.

Chen, C., Chen, C. and Hoang, T. (2016), "Role of concrete confinement of wide-flange structural steel shape in steel reinforced concrete columns under cyclic loading", *Eng. Strct.*, **110**, 79-87.

Chinese Standard (1996), Specifications of testing methods for seismic resistant buildings (JGJ101-96); China Architecture & Building Press, Beijing, China. [In Chinese]

Chinese Standard (2010), Code for Seismic Design of Buildings(GB50011-2010); China Plan Press, Beijing, China. [In Chinese]

Lagaros, N.D. and Magoula, E. (2013), "Life-cycle cost assessment of mid-rise and high-rise steel and steel-reinforced concrete composite minimum cost building designs", *Struct. Des. Tall Special Build.*, **22**, 954-974.

Ma, H., Li, S., Li, Z., Liu, Y., Dong, J. and Zhang, P. (2018), "Shear behavior of composite frame inner joints of SRRC column-steel beam subjected to cyclic loading", *Steel Compos. Struct., Int. J.*, **27**(4), 495-508.

Orr, J.J., Ibell, T.J., Darby, A.P. and Evernden, M. (2014), "Shear behaviour of non-prismatic steel reinforced concrete beams", *Eng. Struct.*, **71**, 48-59.

Pisano, A.A., Fuschi, P. and De Domenico, D. (2013), "Peak loads and failure modes of steel-reinforced concrete beams: Predictions by limit analysis", *Eng. Struct.*, **56**, 477-488.

Shanmugam, N.E. and Lakshmi, B. (2001), "State of the art report on steel-concrete composite columns", *J. Constr. Steel Res.*, **57**(10), 1041-1080.

Wang, Q., Shi, Q. and Tian, H. (2015), "Seismic behavior of steel reinforced concrete (CES) joints with new-type section steel under cyclic loading", *Steel Compos. Struct., Int. J.*, **19**(6), 1561-1580.

Wang, Q., Shi, Q. and Tian, H. (2016), "Experimental study on shear capacity of SRC joints with different arrangement and sizes of cross-shaped steel in column", *Steel Compos. Struct., Int. J.*, **21**(2), 267-287.

Wang, J., Lu, J., Zhang, H. and Zhao, C. (2018), "Experimental investigation on seismic performance of endplate composite joints to CFST columns", *J. Constr. Steel Res.*, **145**, 352-367.

Xiang, P., Su, Y., Wang, H. and Wan, Y. (2017), "Experimental investigation on joints between steel-reinforced concrete T-shaped column and reinforced concrete beam under bidirectional low-cyclic reversed loading", *Adv. Struct. Eng.*, **20**(3), 446-460.

Xu, J., Chen, Z., Chen, Y. and Xue, J. (2015), "Earthquake Damage Evaluation of T-Shaped CES Composite Column-Steel Beams in 3D Connection Joints", *Adv. Struct. Eng.*, **18**(5), 701-713.

Yan, C., Yang, D., Ma, Z. and Jia, J. (2017), "Hysteretic model of SRUHSC column and CES beam joints considering damage effects", *Mater. Struct.*, **50**, 1-13.

Zhang, J. and Jia, J. (2016), “Experimental study on seismic behavior of composite frame consisting of CES beams and SRUHSC columns subjected to cyclic loading”, *Constr. Build. Mater.*, **125**, 1055-1065.

CC